AGU PUBLICATIONS

Geophysical Research Letters

RESEARCH LETTER
10.1002/2016GL068168

Key Points:
- The Chichi-jima earthquake occurred within the mantle transition zone
- The 660 km phase boundary is locally depressed to 690 km depth
- The Izu-Bonin slab is folding within the mantle transition zone

Supporting Information:
- Supporting Information S1

Correspondence to:
R. W. Porritt,
rporritt@usc.edu

Citation:
Porritt, R. W., and S. Yoshioka (2016), Slab pileup in the mantle transition zone and the 30 May 2015 Chichi-jima earthquake, *Geophys. Res. Lett.*, *43*, 4905–4912, doi:10.1002/2016GL068168.

Received 20 OCT 2015
Accepted 1 MAY 2016
Accepted article online 5 MAY 2016
Published online 18 MAY 2016

Slab pileup in the mantle transition zone and the 30 May 2015 Chichi-jima earthquake

Robert W. Porritt[1,2] and Shoichi Yoshioka[1]

[1]Research Center for Urban Safety and Security, Kobe University, Kobe, Japan, [2]Now at Department of Geosciences, University of Arizona, Tucson, Arizona, USA

Abstract The 30 May 2015 Chichi-jima M8 earthquake is one of the largest deep focus earthquakes ever recorded and its depth of 682 km puts it near the base of the mantle transition zone. Before source mechanisms and slip models of this earthquake can be reliably assessed, a better understanding of the tectonic setting and structures of the region near the origin is required. Here we present evidence from receiver functions, a method of isolating subsurface material contrast with converted seismic waves, that the earthquake initiated within the upper mantle transition zone, above a significantly depressed 660 km phase boundary. Additionally, we observe multiple conversions within and below the transition zone, which we associate with seismic waves passing into and out of segments of the subducting Pacific plate. From this, we infer slab material is piling up at the base of the transition zone and segments are penetrating into the lower mantle.

1. Introduction

Deep earthquakes provide rare insights into important processes at the base of the upper mantle. The 30 May 2015 M8 Chichi-jima earthquake (Figure 1) occurred near the base of the mantle transition zone with an oblique normal faulting mechanism (U.S. Geological Survey (USGS) Earthquake Hazards Program) and is among the largest deep focus earthquakes recorded in the past 30 years. Estimates of the exact depth vary, but the range is from a minimum depth of 660 km to a maximum depth of 696 km (USGS Earthquake Hazards Program and Japan Meteorological Agency (JMA)), and for this analysis we use the JMA estimate of 682 km depth. These estimates are deeper than the nominal base of the mantle transition zone at 660 km [e.g., *Dziewonski and Anderson*, 1981; *Kennett and Engdahl*, 1991], which is thought to be the deepest region in which earthquakes can occur. However, this seismic discontinuity can be depressed by ~10–25 km in the presence of cold, and possibly hydrous, material brought down by subduction [e.g., *Ghosh et al.*, 2013]. Here we show that the Chichi-jima earthquake occurred immediately above a significantly depressed 660 km phase boundary and that the subduction of the Pacific plate in this region is folded over on itself above a low viscosity channel.

The mantle transition zone refers to the pressure/depth range where olivine ($(Mg,Fe)_2SiO_4$) undergoes a phase transition into its high pressure and temperature polymorphs of primarily wadsleyite and ringwoodite before its transition into lower mantle perovskite. The phase transition to wadsleyite occurs at ~410 km (pressure of ~13 GPa), which then transitions to ringwoodite at ~520 km (pressure of ~18 GPa), and then transitions to perovskite plus magnesiowüstite at ~660 km depth (pressure of ~23 GPa) [e.g., *Dziewonski and Anderson*, 1981]. Globally averaged seismology studies suggest these boundaries are fairly consistent in depth [e.g., *Anderson and Bass*, 1986], but the specific depth of the transition is a function of the Clapeyron slope and temperature anomaly. High temperature and pressure experimental studies vary significantly on viable values for this slope, but at the extremes, this value can range from −3.2 to 0 MPa/K [*Litasov et al.*, 2005] for the 660 km phase transition, with the most negative values reflecting the effect of hydrous phases. Assuming a linear relationship between depth and pressure of 25 km/GPa, a temperature anomaly of 300 K for the slab, and a Clapeyron slope of −0.4 MPa/K, the 660 km phase transition can be depressed to 663 km depth, but with a Clapeyron slope of −3.2 MPa/K, which would require hydrous phases, this phase transition occurs at 684 km depth.

Understanding the phase transition from ringwoodite to perovskite plus magnesiowüstite has important consequences for geodynamic modeling of the subduction process and corresponding surficial processes. The transition is associated with a change in viscosity [e.g., *Mitrovica and Forte*, 2004], which in some cases causes a slab to change its inclination from a vertically descending body to a flat lying body near the

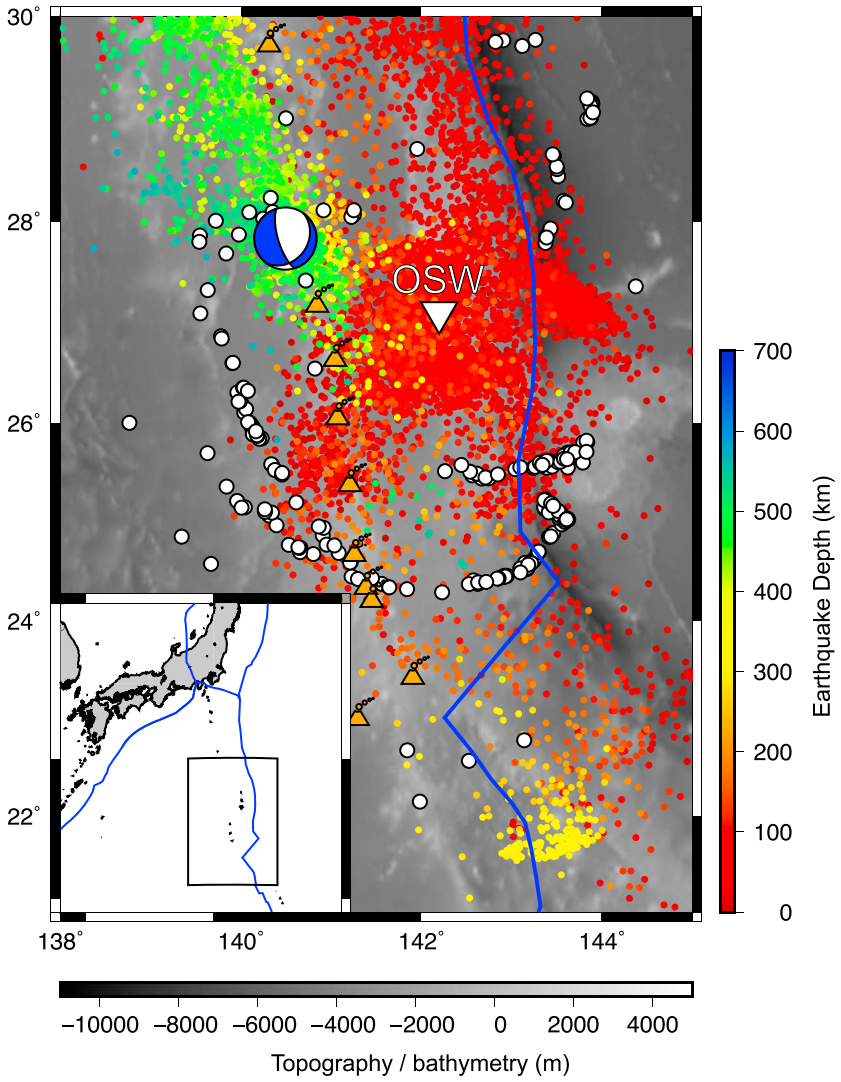

Figure 1. Location map of the Chichi-jima earthquake. Grayscale background indicates topography and bathymetry. Previous earthquakes from the JMA catalog (1998–2014) plotted as circles with color indicating depth. The 30 May 2015 Chichi-jima earthquake plotted as its focal mechanism in lower hemisphere projection (compressional quadrants in blue). White inverted triangle indicates the F-net seismic station OSW. White circles with black outlines indicate piercing points of receiver functions at 660 km depth. Orange triangles indicate active volcanoes along the arc. Blue lines are the plate boundaries. Inset map depicts larger scale region with coastlines of Japan, plate boundaries, and the rectangle indicates the zoomed in region.

660 km phase transition. This change in the slab pull force interacts with trench movement and initial slab dip to affect the overall slab geometry. At depth, seismic images suggest some, but not all, slabs penetrate the 660 km phase boundary and descend to the core-mantle boundary [*Ritsema et al.*, 2011; *Obayashi et al.*, 2013; *Simmons et al.*, 2010; *Lekic and Romanowicz*, 2011]. This has led to the suggestion that the 660 km phase boundary acts as a temporary barrier and as more subducting material builds up, eventually the slab is able to descend deeper by penetrating the barrier. However, geodynamic simulations of this process are highly sensitive to initial subduction conditions, the effective Clapeyron slope, the viscosity structure, trench advance or retreat, and other less quantifiable conditions such as the presence of metastable olivine or water [e.g., *Torii and Yoshioka*, 2007; *Yoshioka and Naganoda*, 2010].

The Izu-Bonin arc is the type example of a flat lying slab through the transition zone. Global and regional scale tomography models typically image a large, nearly horizontal, high velocity anomaly within the transition zone west of the Izu-Bonin trench [*Obayashi et al.*, 2013]. The eastern edge of this anomaly connects with a steeply dipping high velocity anomaly, coincident with significant seismicity used to define the

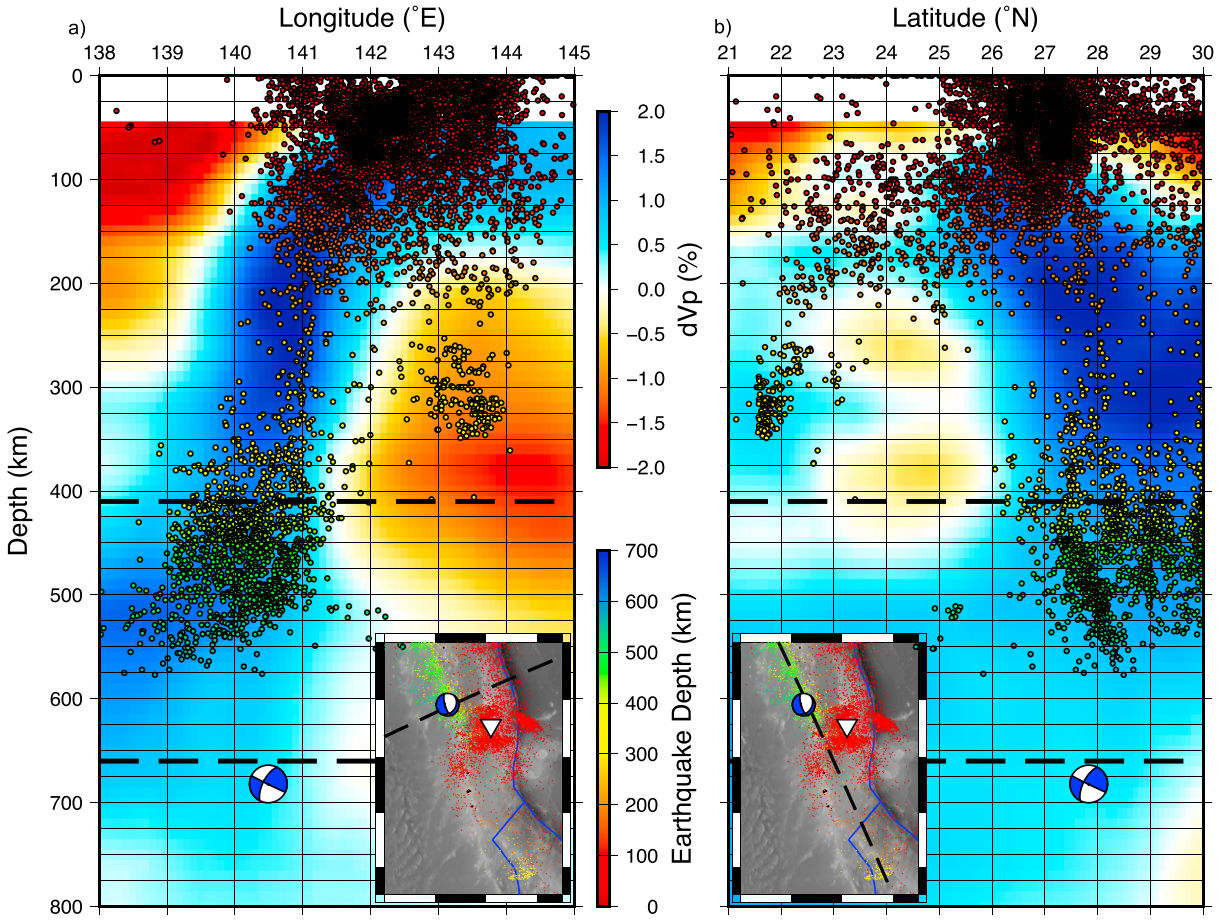

Figure 2. Comparison of previous seismicity from the JMA catalog and the relative velocity structure of the GAP_P4 velocity model [*Obayashi et al.*, 2013]. Colored dots indicate earthquakes with their depth, dashed black lines indicate the top and bottom of the transition zone, and the Chichi-jima earthquake is plotted with its depth-projected focal mechanism. (a) All JMA catalog earthquakes (1998–2014) in the region are plotted against longitude and the location of the tomography is indicated in the inset map. (b) All JMA catalog earthquakes (1998–2014) are plotted against latitude and the location of the tomography is indicated in the inset map.

Wadati-Benioff zone of the Pacific slab (Figure 2). Previous studies have investigated this region with reflected seismic waves and found the 660 km seismic discontinuity is deepened by ~20–60 km [*Vidale and Benze*, 1992; *Wicks and Richards*, 1993], and these observations are reflected in our receiver function data. Therefore, we can infer there is relatively cold and at least partially hydrous material at the base of the transition zone in this region. However, these previous studies focused on seismic waves converted near the source of deep focus earthquakes and only inform us about the ringwoodite-perovskite transition and not about processes or structures within the transition zone.

2. Source Region Structure

Figure 2 shows the seismicity in the region from the Japan Meteorological Agency (JMA) overlain on cross sections through the GAP_P4 *P* wave velocity model [*Obayashi et al.*, 2013] along a west to east profile (Figure 2a) and a south to north profile (Figure 2b). The high velocity portions of the upper mantle largely coincide with the earthquake locations as expected for the Wadati-Benioff zone [*Brodholt and Stein*, 1988]. However, the Chichi-jima earthquake occurred at the edge of the high velocity anomaly and is isolated from the Wadati-Benioff zone because it is ~80–100 km deeper than the nearest other deep focus earthquakes. Therefore, this earthquake is not part of the Wadati-Benioff zone seismicity and its relationship to the slab and transition zone is unclear.

In order to investigate the tectonic setting and structures in which the earthquake occurred, we calculate 237 *P* to *S* receiver functions (PRFs) [*Langston*, 1977; *Vinnik*, 1977] at the nearby one and only seismic station OSW,

operated by the National Research Institute for Earth Science and Disaster Prevention (NIED) as part of the F-Net broadband network. For this analysis, we use a Gaussian filter of 1.0 and a water level deconvolution where the water level is determined based on the peak of the prearrival noise spectrum. Tests for the robustness of this choice are shown in Figures S1 through S21 in the supporting information. Higher frequency Gaussian filters, such as 2.0, contain several conversions at mantle depths that disappear at lower frequency Gaussian filters. Lower frequency Gaussian filters, such as 1.0 and 0.5, do not show significant differences between a water level style deconvolution and an iterative, time domain, deconvolution, suggesting this choice does not affect our results significantly. Finally, the specific choice of the water level (i.e., minimum frequency domain amplitude in the denominator) relative to the peak noise is tested at 100.1%, 101%, and 110% and no significant difference is observed.

The choice of velocity model used in the time-to-depth migration can have a significant effect on the inferred structure at upper mantle depths. Therefore, we test the results of the migration with four different 1-D velocity models and one 3-D model in Figure S22. This figure shows little variation in the 1-D mean stacked receiver function in the upper crust and lithosphere but up to ~15 km variation in transition zone structure. We choose to use the 3-D GyPSuM model [*Simmons et al*., 2010] for this analysis because it contains both *P* and *S* wave velocities on the same scales and is defined globally. This migration is implemented by initially mapping the raypaths with the AK135 global 1-D velocity model [*Kennett et al*., 1995] and updating the path with a single iteration through GyPSuM [*Simmons et al*., 2010]. The 660 km depth piercing points indicated in Figure 1 show the region near the earthquake focus is well sampled by our data set.

Receiver functions are sensitive to velocity contrasts along the raypath, such as those at the Moho (crust-mantle boundary), the lithosphere-asthenosphere boundary, and the top and bottom of the mantle transition zone [*Zhu and Kanamori*, 2000; *Levander and Miller*, 2012; *Thompson et al*., 2011]. Velocity increases with depth, such as expected for the ringwoodite to perovskite phase transition or the top of a slab, appear as positive PRF amplitudes. Due to their ability to resolve velocity contrasts across multiple scales from the upper mantle to the crust, receiver functions have grown significantly in popularity in recent years [e.g., *Kawakatsu and Yoshioka*, 2011; *Miller et al*., 2014; *Porritt et al*., 2015]. Therefore, we compare the focus of the Chichi-jima earthquake to PRF amplitudes to infer where the earthquake occurred relative to the slab and the mantle transition zone.

3. Results

Figure 3 shows the spatially mapped PRFs in relation to the earthquakes also shown in Figure 2. We identify five horizons, (a) to (e), based on the alignment of positive pulses. The shallowest horizon (a) is observed between 325 and 375 km depth. This horizon is too shallow for the top of the transition zone and its dip suggests it may be a multiple of a shallower conversion. However, it is notable that the cloud of deep seismicity begins immediately below this horizon. Horizon (b) is at ~425 km depth and is therefore a candidate for the top of the mantle transition zone. Horizon (c) is within the middle of the transition zone and is deepest under the main patch of seismicity. Horizon (d) is our pick for the base of the mantle transition zone and we observe it significantly deepened under the inferred slab and near the Chichi-jima earthquake. Horizon (e) is deeper than the base of our inferred transition zone and therefore this conversion represents an anomalous feature in the uppermost lower mantle.

We summarize the structural variation in Figure 4 by focusing on receiver functions with raypaths which pass near the Chichi-jima earthquake and on the larger scale tomographic imaging. This comparison shows agreement between the two imaging methods. The tomographic slice alone shows a narrow, steeply dipping slab above the transition zone and a thick, broad, high velocity anomaly within the transition zone. The receiver functions show the 410 km discontinuity is slightly deepened and the 660 km seismic discontinuity is significantly depressed. The receiver functions also show a midtransition zone positive conversion and a subtransition zone positive conversion. These conversions are highlighted in the inset to the left which shows a stack of receiver functions with a back azimuth toward the northwest. Finally, we observe a positive peak at ~750 km depth. This is too deep for a candidate for the base of the transition zone and we therefore infer this is the top of the high-viscosity lower mantle. The separation between this conversion and the base of the transition zone allows for a narrow, low viscosity channel.

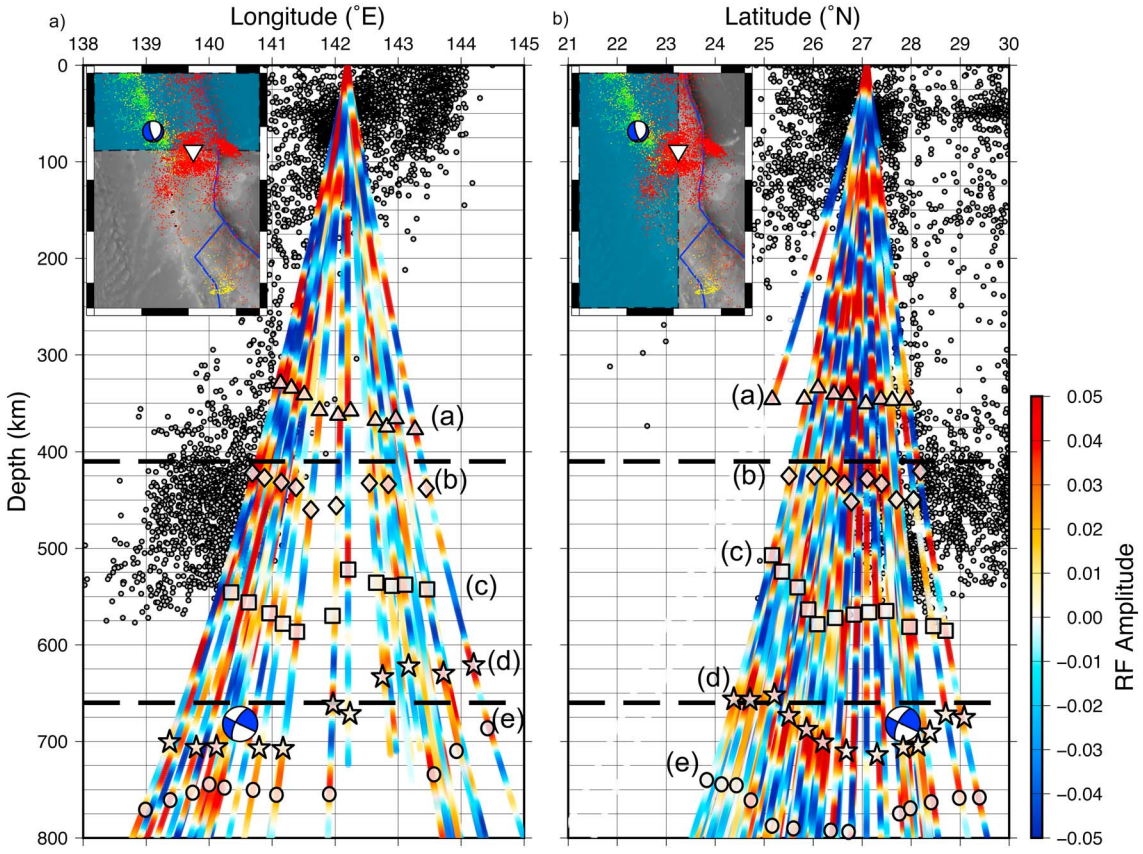

Figure 3. Comparison of previous seismicity from the JMA catalog and the receiver function amplitudes. Gray dots indicate earthquakes, dashed black lines indicate the top and bottom of the transition zone, and the Chichi-jima earthquake is plotted with its map view focal mechanism. (a) All JMA catalog earthquakes (1998–2014) and receiver functions north of station OSW are plotted against longitude. Horizons (a)–(e) indicate positive conversion points as mentioned in the text. (b) All earthquakes JMA catalog (1998–2014) and receiver functions west of station OSW are plotted against latitude. The inset maps indicate the regions from which the receiver functions are gathered in blue.

4. Discussion

The upper mantle conversions observed for receiver functions passing near the 30 May 2015 Chichi-jima earthquake hypocenter display a series of positive pulses associated with structure that may be expected but at depths which suggest a complex history of subduction dynamics. A conversion near 410 km depth appears deeper than would be expected for an oceanic plate subducting through the top of the transition zone. A midtransition zone positive conversion is observed at greater depth than the wadsleyite-ringwoodite transition, and we therefore interpret it as a structural feature rather than a phase transition. The base of the mantle transition zone is observed to ~690 km depth, consistent with a relatively cold, and possibly hydrous, region. Finally, we observe a strong deep conversion at ~750 km depth, significantly below the base of the transition zone.

The series of conversions suggests the slab in this region is folded over upon itself. This structure forms when a slab dips steeply as it descends toward the base of the transition zone. Once it reaches the base of the transition zone, the slab overturns and flattens with the top of the slab downward. This leads to trench advance as the slab deposits on the viscosity contrast across the 660 km seismic discontinuity until trench retreat initiates and reverses the system. As the oceanic plate continues to subduct, it folds back and lies on top of the older slab, now with the slab top up. This results in an apparently thicker slab pile in the mantle transition zone, which eventually builds enough negative buoyancy to penetrate into the lower mantle [e.g., *Christensen*, 1996].

Each one of the main conversions provides a different piece of information to support this interpretation. The shallow three conversions labeled in Figure 4 as P1, P2, and P3 are relatively high amplitude but are clearly above the transition zone. They are regularly spaced and have constant dip between them, suggesting they

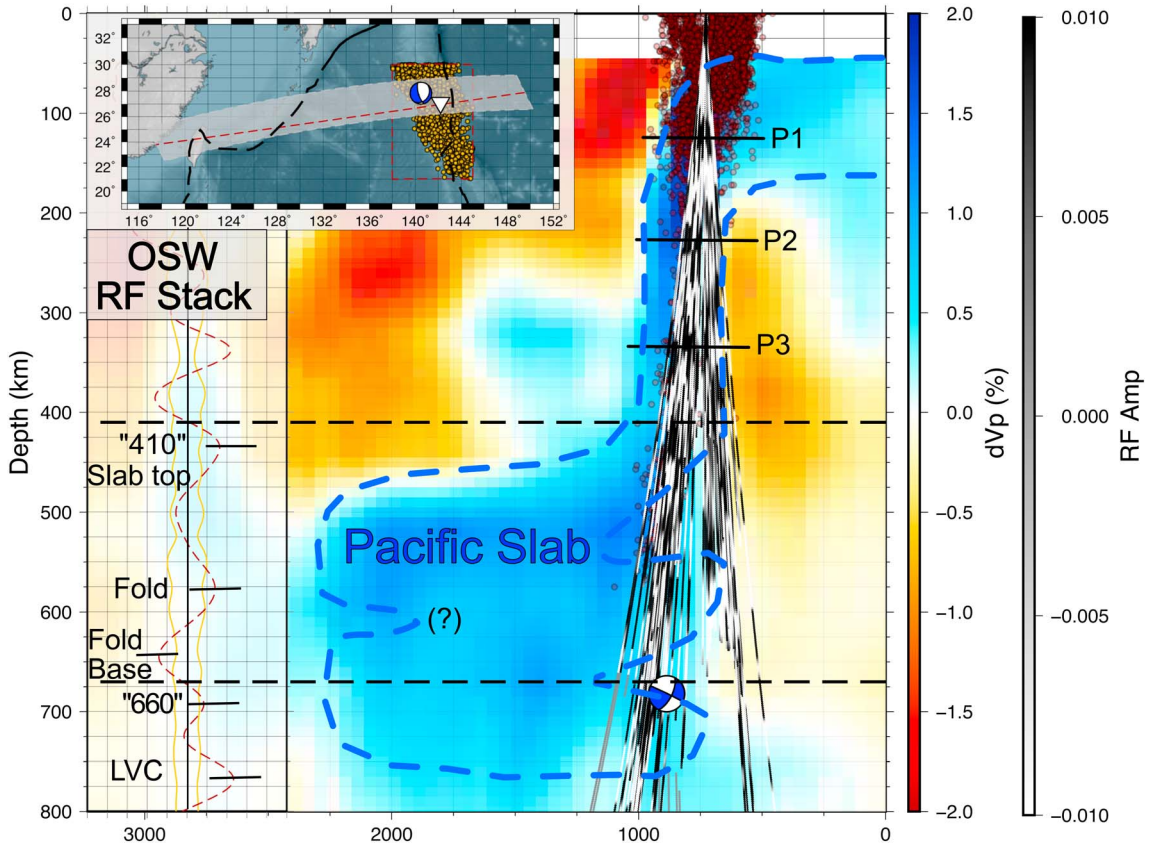

Figure 4. Interpretation of receiver function and complementary data. Red to blue background is the relative *P* wave velocity of the GAP_P4 global tomography model of *Obayashi et al.* [2013] along a profile indicated in a red dashed line in the inset map to the upper left. White to gray lines indicate receiver functions at station OSW projected along the red line in the inset map, limited to the white shaded region along the profile. Dark red dots indicate earthquakes within the same band, projected onto the profile. Blue dashed lines indicate the interpreted slab geometry. P1, P2, and P3 are receiver function conversions which are suspected as multiples or shallow slab conversions. The blue beach ball is the Chichi-jima earthquake focal mechanism projected at depth. The left hand red dashed line on a transparent white background is the stacked receiver functions at station OSW for receiver functions with a northwest incidence and uncertainty based on a bootstrap resampling. The strong positive conversions are marked for the 410 km discontinuity, the slab fold, the 660 km discontinuity, and the base of the inferred low viscosity channel. The southwestward extent of the slab fold (indicated by (?)) is inferred from the eastern structure. Map view gold dots indicate earthquakes within the limited region of Figure 1.

may be multiples. The conversion near 410 km depth, also labeled (b) in Figure 3, is deeper than would be expected for the olivine to wadsleyite conversion with a positive Clapeyron slope in the presence of cooler mantle temperature but does not appear to be a multiple. The GAP_P4 model, as shown in Figures 2 and 4, indicates that this conversion is within the subducting slab, and we therefore infer two processes are responsible for the apparently deepened 410 km discontinuity. First, the presence of a hydrated lens of wadsleyite could reduce the velocity contrast across the transition zone and above the slab, thereby masking the 410 km discontinuity [*Schmerr and Garnero*, 2007]. Second, a slab core of metastable olivine could cause the phase transition within the slab to be located at greater depth [e.g., *Yoshioka et al.*, 2015] and the structural dip of the slab may be responsible for the P3 layer, if it is not a multiple.

There are two major conversions within the transition zone based on the stack of PRFs passing near the earthquake origin: a positive labeled as a slab fold at ~575 km and the other is a negative conversion labeled as a fold base near 640 km depth. The shallower positive conversion is deeper than the ~520 km phase transition depth and this boundary is not often associated with clear seismic phase conversions. This leads to a structural interpretation rather than a mineralogical explanation. Tracking the positive and negative conversion pairs through the transition zone suggests a region at ~640 km depth where the upward traveling rays enter the slab (negative fold base conversion), then exit and reenter the slab around 600 km (near the "fold" label), exit the slab again by ~520 km depth, and finally reenter the slab at ~480 km depth. This series of conversions suggests the apparent thickening of the slab through the transition zone is a result of the slab doubled over

upon itself, which is a geometry that could have developed during the ~130–140 Myr subduction history of the Izu-Bonin system [*Syracuse and Abers*, 2006].

The base of the transition zone is deepened from its nominal depth of 660 km to ~690 km depth. This is consistent with previous studies [e.g., *Vidale and Benze*, 1992; *Wicks and Richards*, 1993] which have shown a deepened 660 km seismic discontinuity in this region. Our test of varying the model for the time-to-depth migration shows up to ~15 km variability, but this still requires the boundary to be deepened by 15–30 km. This would require a Clapeyron slope of −2 to −3.2 MPa/K, assuming a ~300 K thermal anomaly. A large negative Clapeyron slope is most readily associated with the presence of water [e.g., *Ghosh et al*., 2013] possibly brought down by the subducting plate. In our interpretation of the slab multiply folded over upon itself, it is possible the water is well distributed throughout the slab or that metastable olivine is present to depress the apparent transition zone boundary.

The deepest conversion imaged is at ~750 km, which is deeper than is plausible for the base of the transition zone. Rather, recent studies have argued for a midmantle increase in viscosity at ~1000 km depth [*Ballmer et al*., 2015; *Rudolph et al*., 2015] and a low viscosity zone immediately at the phase transition, which might be related to grain size reduction associated with the phase transition from ringwoodite to perovskite plus magnesiowüstite [e.g., *Yoshioka and Naganoda*, 2010]. We therefore infer that this positive conversion represents the base of a low viscosity region. Below this conversion, viscosity may increase to ~1000 km depth where seismic evidence suggests some slabs stagnate [e.g., *Ballmer et al*., 2015]. Above this conversion, we interpret a narrow low viscosity channel as implemented in the modeling work of *Yoshioka and Naganoda* [2010]. Both a low viscosity channel at the base of the transition zone and a high-viscosity lower mantle are factors that increase slab stagnation at the 660 km discontinuity [e.g., *Yoshioka and Naganoda*, 2010].

Modeling of the rupture of the Chichi-jima earthquake is consistent with this interpretation. *Ye et al*. [2016] show that this earthquake has a two-stage rupture process and is intermediate in rupture style between brittle failure and ductile failure. This modeling suggests that this earthquake is similar to crustal faulting but with very limited aftershock activity [*Ye et al*., 2016]. The structural imaging presented here indicates the earthquake occurred immediately above the base of the depressed transition zone, near the top of an isolated limb of the slab. The limited aftershock activity may be a consequence of an anomalously hydrous slab or a relatively large proportion of metastable olivine within this limb, both of which could be responsible for the depressed base of the transition zone.

5. Conclusion

The 30 May 2015 Chichi-jima earthquake is among the largest deep focus earthquakes recorded in the past 30 years. This earthquake is ~100 km deeper than previous seismicity of deep focus earthquakes in the region and seismic tomographic velocity imaging indicates it occurred within a broad high velocity anomaly. Our new receiver function data indicate the base of the mantle transition zone is at 690 km depth, 8 km below the 682 km hypocentral depth of the earthquake, and we observe significant conversions above and below the base of the transition zone. We infer from this that the slab is piling up at the base of the transition zone and the Chichi-jima earthquake occurred in a deep limb of the slab immediately above the base of the transition zone.

Acknowledgments

We thank the NIED for the seismic waveform data presented in Figures 3 and 4. We thank the JMA for the earthquake locations in Figures 1–4. We thank M. Obayashi for sharing the GAP_P4 model and N. Simmons for the GyPSuM model accessed via the IRIS Earth Model Collaboration website. We thank two anonymous reviewers for their critical comments used to improve this manuscript. Early processing of the waveform data was done with FuncLab [*Eagar and Fouch*, 2012]. All figures made with GMT. Funding for R.W. Porritt was provided by NSF-EAR Postdoctoral Fellowship 1249776 and Kobe University Research Center for Urban Safety and Security. USGS Earthquake Hazards Program: http://earthquake.usgs.gov/earthquakes/eventpage/us20002ki3 (accessed 27 August 2015). JMA bulletin on Chichi-jima earthquake: http://www.jma.go.jp/jma/press/1505/31d/201505311600.pdf (accessed 27 August 2015). Receiver functions and an updated version of Funclab can be requested by email to the corresponding author rwporritt@gmail.com

References

Anderson, D. L., and J. D. Bass (1986), Transition region of the Earth's upper mantle, *Nature*, *320*(6060), 321–328, doi:10.1038/320321a0.

Ballmer, M., N. Schmerr, T. Nakagawa, and J. Ritsema (2015), Compositional mantle layering revealed by slab stagnation at ~1000-km depth, *Sci. Adv.*, *1*(11), e1500815.

Brodholt, J., and S. Stein (1988), Rheological control of Wadati-Benioff zone seismicity, *Geophys. Res. Lett.*, *15*(10), 1081–1084, doi:10.1029/GL015i010p01081.

Christensen, U. R. (1996), The influence of trench migration on slab penetration into the lower mantle, *Earth Planet. Sci. Lett.*, *140*(1–4), 27–39, doi:10.1016/0012-821X(96)00023-4.

Dziewonski, A. M., and D. L. Anderson (1981), Preliminary reference Earth model, *Phys. Earth Planet. Inter.*, *25*(4), 297–359, doi:10.1016/0031-9201(81)90046-7.

Eagar, K. C., and M. J. Fouch (2012), FuncLab: A MATLAB interactive toolbox for handling receiver function datasets, *Seismol. Res. Lett.*, *83*(3), 596–603, doi:10.1785/gssrl.83.3.596.

Ghosh, S., E. Ohtani, K. D. Litasov, A. Suzuki, D. Dobson, and K. Funakoshi (2013), Effect of water in depleted mantle on post-spinel transition and implication for the 660 km seismic discontinuity, *Earth Planet. Sci. Lett.*, *371–372*, 103–111, doi:10.1016/j.epsl.2013.04.011.

Kawakatsu, H., and S. Yoshioka (2011), Metastable olivine wedge and deep dry cold slab beneath southwest Japan, *Earth Planet. Sci. Lett.*, *303*(1–2), 1–10, doi:10.1016/j.epsl.2011.01.008.
Kennett, B. L. N., and E. R. Engdahl (1991), Traveltimes for global earthquake location and phase identification, *Geophys. J. Int.*, *105*(2), 429–465, doi:10.1111/j.1365-246X.1991.tb06724.x.
Kennett, B. L. N., E. R. Engdahl, and R. Buland (1995), Constraints on seismic velocities in the Earth from traveltimes, *Geophys. J. Int.*, *122*(1), 108–124, doi:10.1111/j.1365-246X.1995.tb03540.x.
Langston, C. (1977), Corvallis, Oregon, crustal and upper mantle receiver structure from teleseismic *P*-waves and *S*-waves, *Bull. Seismol. Soc. Am.*, *67*(3), 713–724.
Lekic, V., and B. Romanowicz (2011), Inferring upper-mantle structure by full waveform tomography with the spectral element method, *Geophys. J. Int.*, *185*(2), 799–831, doi:10.1111/j.1365-246X.2011.04969.x.
Levander, A., and M. S. Miller (2012), Evolutionary aspects of lithosphere discontinuity structure in the western U.S., *Geochem. Geophys. Geosyst.*, *13*, Q0AK07, doi:10.1029/2012GC004138.
Litasov, K., E. Ohtani, A. Sano, A. Suzuki, and K. Funakoshi (2005), In situ X-ray diffraction study of post-spinel transformation in a peridotite mantle: Implication for the 660-km discontinuity, *Earth Planet. Sci. Lett.*, *238*, 311–328, doi:10.1016/j.epsl.2005.08.001.
Miller, M. S., P. Zhang, and J. F. Dolan (2014), Moho structure across the San Jacinto fault zone: Insights into strain localization at depth, *Lithosphere*, *6*(1), 43–47, doi:10.1130/L295.1.
Mitrovica, J. X., and A. M. Forte (2004), A new inference of mantle viscosity based upon joint inversion of convection and glacial isostatic adjustment data, *Earth Planet. Sci. Lett.*, *255*(1–2), 177–189, doi:10.1016/j.epsl.2004.06.005.
Obayashi, M., J. Yoshimitsu, G. Nolet, Y. Fukao, H. Shiobara, H. Sugioka, H. Miyamachi, and Y. Gao (2013), Finite frequency whole mantle *P* wave tomography: Improvement of subducted slab images, *Geophys. Res. Lett.*, *40*, 5652–5657, doi:10.1002/2013GL057401.
Porritt, R. W., M. S. Miller, and F. A. Darbyshire (2015), Lithospheric architecture beneath Hudson Bay, *Geochem. Geophys. Geosyst.*, *16*, 2262–2275, doi:10.1002/2015GC005845.
Ritsema, J., A. Deuss, H. J. van Heijst, and J. H. Woodhouse (2011), S40RTS: A degree-40 shear-velocity model for the mantle from new Rayleigh wave dispersion, teleseismic traveltime and normal-mode splitting function measurements, *Geophys. J. Int.*, *184*(3), 1223–1236, doi:10.1111/j.1365-246X.2010.04884.x.
Rudolph, M. L., V. Lekic, and C. Lithgow-Bertelloni (2015), Viscosity jump in Earth's mid-mantle, *Science*, *350*(6266), 1349–1352, doi:10.1126/science.aad1929.
Schmerr, N., and E. J. Garnero (2007), Upper mantle discontinuity topography from thermal and chemical heterogeneity, *Science*, *318*(623), doi:10.1126/science.1145962.
Simmons, N. A., A. M. Forte, L. Boschi, and S. P. Grand (2010), GyPSuM: A joint tomographic model of mantle density and seismic wave speeds, *J. Geophys. Res.*, *115*, B12310, doi:10.1029/2010JB007631.
Syracuse, E. M., and G. A. Abers (2006), Global compilation of variations in slab depth beneath arc volcanoes and implications, *Geochem. Geophys. Geosyst.*, *7*, Q05017, doi:10.1029/2005GC001045
Thompson, D. A., G. Helffrich, I. D. Bastow, J.-M. Kendall, J. Wookey, D. W. Eaton, and D. B. Snyder (2011), Implications of a simple mantle transition zone beneath cratonic North America, *Earth Planet. Sci. Lett.*, *312*(1–2), 28–36, doi:10.1016/j.epsl.2011.09.037.
Torii, Y., and S. Yoshioka (2007), Physical conditions producing slab stagnation: Constraints of the Clapeyron slope, mantle viscosity, trench retreat, and dip angles, *Tectonophysics*, *445*, 200–209, doi:10.1016/j.tecto.2007.08.003.
Vidale, J. E., and H. M. Benze (1992), Upper-mantle seismic discontinuities and the thermal structure of subduction zones, *Nature*, *356*(6371), 678–683, doi:10.1038/356678a0.
Vinnik, L. P. (1977), Detection of waves converted from *P* to SV in mantle, *Phys. Earth Planet. Inter.*, *15*(1), 39–45, doi:10.1016/0031-9201(77)90008-5.
Wicks, C. W., and M. A. Richards (1993), A detailed map of the 660-kilometer discontinuity beneath the Izu-Bonin subduction zone, *Science*, *261*(5127), 1424–1427, doi:10.1126/science.261.5127.1424.
Ye, L., T. Lay, Z. Zha, H. Kanamori, and J.-L. Hao (2016), The isolated ~680 km deep 30 May 2015 M_w 7.9 Ogasawara (Bonin) Islands earthquake, *Earth Planet. Sci. Lett.*, *433*, 169–179, doi:10.1016/j.epsl.2015.10.049.
Yoshioka, S., and A. Naganoda (2010), Effects of trench migration on fall of stagnant slabs into the lower mantle, *Phys. Earth Planet. Inter.*, *183*, 321–329, doi:10.1016/j.pepi.2010.09.002.
Yoshioka, S., Y. Torii, and M. R. Riedel (2015), Impact of phase change kinetics on the Mariana slab within the framework of 2-D mantle convection, *Phys. Earth Planet. Inter.*, *240*, 70–81, doi:10.1016/j.pepi.2014.12.001.
Zhu, L., and H. Kanamori (2000), Moho depth variation in southern California from teleseismic receiver functions, *J. Geophys. Res.*, *105*(B2), 2969–2980, doi:10.1029/1999JB900322.